 CMES, vol.21, no.2, pp.157-175, 2007

Acoustic Scattering in Prolate Spheroidal Geometry via Vekua Tranformation – Theory and Numerical Results

L.N. Gergidis, D. Kourounis, S. Mavratzas and A. Charalambopoulos [1]

Abstract: A new complete set of scattering eigensolutions of Helmholtz equation in spheroidal geometry is constructed in this paper. It is based on the extension to exterior boundary value problems of the well known Vekua transformation pair, which connects the kernels of Laplace and Helmholtz operators. The derivation of this set is purely analytic. It avoids the implication of the spheroidal wave functions along with their accompanying numerical deficiencies. Using this novel set of eigensolutions, we solve the acoustic scattering problem from a soft acoustic spheroidal scatterer, by expanding the scattered field in terms of it. Two approaches concerning the determination of the expansion coefficients are extensively studied in terms of their numerical and convergence properties. The first one minimizes the L^2-norm of a suitably constructed error function and the second one relies on collocation techniques. The robustness of these approaches is established via the adoption of arbitrary precision arithmetic.

Keyword: Prolate Spheroid; Acoustic Scattering; Vekua Transformation; Arbitrary Precision; L^2-norm Minimization; Collocation; Mathematical Modeling; Special Functions; Scientific Computing.

1 Introduction

The investigation of interior and exterior boundary value problems formulated in spheroidal geometry has been receiving increased attention from both theoretical and application point of view. To a large extent, this is due to the fact that a wide variety of inclusions or inhomogeneities, disturbing wave propagation and encountered in real life applications, can be modeled very accurately by either prolate or oblate spheroidal bodies. In [Kong, Li, Leong, and Kooi (1999)], [Kourounis, Charalambopoulos, and Fotiadis (2001)] the authors model the human head as a prolate spheroidal body, while studying the electromagnetic interaction between a head and a cellular phone. Scattering processes, by layered spheroidal structures, simulating the kidney-stone system are considered in [Charalambopoulos, Dassios, Fotiadis, and Massalas (2001)], [Charalambopoulos, Fotiadis, and Massalas (2002)], [Anagnostopoulos, Mavratzas, Charalambopoulos, and Fotiadis (2003)]. Raindrops, can be modeled as oblate spheroids, for the computation of the rainfall attenuation of microwave signals in satellite telecommunication systems. Rockets, aircraft noses and guided missiles are generally considered to have spheroidal shapes. Relative works concerning burried spheroidal bodies in electromagnetic scattering can be found in [Perruson, Lambert, Lesselier, Dassios, and Charalambopoulos (2000)], [Perruson, Lesselier, Lambert, Bourgeois, Charalambopoulos, and Dassios (2000)], [Charalambopoulos, Dassios, Perruson, and Lesselier (2002)].

The scattering problem of acoustic waves from spheroidal scatterers, constitutes a generalization of the spherical case, and gives birth to models simulating more interesting realistic problems than these "living" in the spherical geometry. A lot of effort has been devoted to the spheroidal scattering problem, especially under the low frequency regime (see references cited in [Charalambopoulos, Dassios, Fotiadis, and Massalas (2001)]). The later approach simplifies the analysis as it permits the investigation of the scattering problem via a sequence of corresponding poten-

[1] Department of Materials Science and Engineering, University of Ioannina, GR 45110 Ioannina, Greece

tial problems referring to the underlying geometry. However, when the dimension of the scatterer is comparable with the wavelength of the incident field, this approach is inadequate. Several works rectify the problem in the resonance region, using either separation of variables or T-matrix techniques [Waterman (1969)], [Zhang and Han (2005)]. In the vast majority of those approaches the well known spheroidal wave functions dominate, which emerge via the spectral investigation of Helmholtz equation in spheroidal coordinates.

It is well known that intermediate numerical implementation is required to construct the aforementioned spheroidal wave functions, which becomes extremely complicated for spheroids with large focal distances and small semiaxes ratio. Drawbacks and fine new achievements on the field of implementation of spheroidal wave functions can be found in [Li, Kang, and Leong (2001)], while analytical shortcuts to exploit spheroidal eigenvectors in solving boundary value problems, are presented in [Charalambopoulos, Fotiadis, Kourounis, and Massalas (2001)].

Apart from the intrinsic numerical difficulty characterizing the construction of the spheroidal wave functions, the solvability of the scattering problem in spheroidal geometry requires a demanding numerical investigation. More precisely, the adopted methodology of expanding the scattering field in terms of spheroidal wave functions, leads to extremely ill-conditioned matrices, involved in the linear systems derived by the satisfaction of the boundary conditions. It is widely recognized, that the 64-bit and 80-bit IEEE floating point arithmetic formats, currently provided and utilized in most computer systems, are inadequate for the inversion of ill-conditioned matrices [Trefethen and Bau (1997)]. This observation does not only concern problems arising in scattering theory but also in several scientific areas such as Experimental Mathematics [Borwein and Bailey (2004)], [Bailey (2004)], Climate Modeling, Atomic System Simulations, Computational Geometry [Shewchuk (1997)] and Number Theory among many others. As already pointed out by other researchers working on computational studies of electromagnetic scattering, the accuracy of the results obtained using conventional 64-bit double precision arithmetic, significantly restrains the range of the wave functions that can be assessed [Barrowes, O'Neil, Grzegorczyk, and Kong (2004)]. Consequently unless a robust methodology is adopted for the numerical treatment of the underlying systems, the numerical results obtained leave a lot to be desired.

In the present work we try to give new prospects in both theoretical and numerical treatment of the acoustic scattering problem from speroidal scatterers. First we introduce a novel pure theoretical approach, avoiding the implication of the spheroidal wave functions and secondly we present a thorough numerical implementation the core of which is based on arbitrary precision facilities. More precisely, our theoretical framework, is inspired by the concepts introduced in [Charalambopoulos and Dassios (2002)], where the famous Vekua transformation pair is adopted, allowing so the construction of Helmholtz equation solutions by tranforming appropriately the corresponding Laplace equation kernel basis functions. The full development of the underlying theory is found in [Vekua (1942)],[Vekua (1967)] and [Vekua (1945)]. In section 2 we extend the aforementioned methodology, to exterior domains, constructing so a complete set of radiating outwards exterior solutions of the Helmholtz equation, constituting an alternative set to the set of spheroidal wave functions. We construct so, a basis set for the Helmholtz equation kernel for exterior problems, in a rather say, quasi-separable form, i.e. as superpositions of separable terms. In section 3, the representative acoustic scattering problem of a plane wave from a soft prolate spheroidal impenetrable scatterer is presented. The formulation of the problem incorporates the representation of the scattered field to be determined, as a superposition of the aforementioned constructed Vekua radiating eigensolutions. This expansion satisfies the appropriate differential equation and remote asymptotics. The boundary condition treatment, leads to a dense algebraic linear system the solution of which provides the expansion coefficients. In section 4, we suggest two different approaches for the dis-

cretization of boundary conditions. The first one is a collocation method while the other achieves an optimal choice of coefficients which minimizes the L^2 norm of the error representing the failure of the boundary condition satisfaction. In section 5, we demonstrate the robustness of those approaches and investigate numerically their convergence properties in appropriate norms. The core of our numerical implementation relies on arbitrary precision facilities, which guarantees the solvability of severely ill-conditioned algebraic linear systems as demonstrated in subsection 5.2. Finally we expose the far-field pattern which usually constitutes the measured quantity in direct scattering.

2 The Vekua Transformation in Spheroidal Geometry

In [Vekua (1942)], [Vekua (1967)], Vekua derived the general one-to-one transformation between the kernel of Laplace and Helmholtz operators, for arbitrary dimension, through the formulae:

$$u(x_1,x_2,...,x_n) = u_0(x_1,x_2,...,x_n) - \int_0^1 u_0(tx_1,tx_2,...,tx_n)t^{\frac{n-2}{2}}\frac{\partial}{\partial t}J_0(kr\sqrt{1-t})dt \quad (1)$$

$$u_0(x_1,x_2,...,x_n) = u(x_1,x_2,...,x_n) + \frac{1}{2}kr\int_0^1 u(tx_1,tx_2,...,tx_n)t^{\frac{n-2}{2}}I_1(kr\sqrt{t(1-t)})\frac{dt}{\sqrt{t(1-t)}} \quad (2)$$

where $u \in ker(\Delta + k^2)$, $u_0 \in ker\Delta$, J_n stands for the Bessel function of order n, I_n denotes the modified Bessel function of order n, x_i with $i = 1,2,..,n$ are the cartesian coordinates and r the Euclidean distance of $\mathbf{r} = (x_1,x_2,\ldots,x_n)$ from the coordinate origin O. The wave number k and the frequency ω of the scattering process are interrelated via the basic relation $k = \omega/c$ where c stands for the velocity of the acoustical waves. Equation (1) gives at first glance, the hope of constructing a family of solutions of Helmholtz equations, from the kernel set of Laplace operator. More precisely, in three dimensional spaces, the first equation of the transformation pair becomes

$$u(\mathbf{r}) = u_0(\mathbf{r}) - \frac{kr}{2}\int_0^1 u_0(t\mathbf{r})J_1(kr\sqrt{1-t})\frac{\sqrt{t}}{\sqrt{1-t}}dt \quad (3)$$

while the second one gives

$$u_0(\mathbf{r}) = u(\mathbf{r}) + \frac{kr}{2}\int_0^1 u(t\mathbf{r})I_1(kr\sqrt{t(1-t)})\frac{dt}{\sqrt{1-t}} \quad (4)$$

where $r = |\mathbf{r}| = ({x_1}^2 + {x_2}^2 + {x_3}^2)^{\frac{1}{2}}$.

The transformation presented above clearly concerns regular, near the origin functions, and concequently refers to solutions of Laplace and Helmholtz equation in interior domains. In [Charalambopoulos and Dassios (2002)] special effort has been devoted to construct an equivalent transformation pair concerning functions regular at infinity, representing solutions of exterior boundary value problems. Although the outcome of the following therein extended analysis, is formally in accordance with the corresponding interior transformation pair, the analytical manipulations however, required for the exploitation of the new tranformation pair, are getting rather cumbersome due to the appearance of a complex contour integration [see Eq.(33) in Charalambopoulos and Dassios (2002)] which is difficult to be implemented in spheroidal geometry. In this work, we follow an alternative approach to acquire Helmholtz equation solutions suitable to describe scattering processes. The later avoids this exterior transformation pair, but modifies instead, in an efficient manner, the results produced via the solutions of the Helmholtz equation which are regular near the origin.

More precisely, in section 3 of [Charalambopoulos and Dassios (2002)] a lot of analysis has been devoted to develop the structure of Helmholtz equation kernel in spheroidal coordinates, with purely analytical means (i.e. without intermediate recurrence numerical schemes), for the case of interior boundary value problems. We are going to exploit this analysis to handle exterior processes instead of alternative tranformation pairs.

Let us consider the prolate spheroidal coordinates μ, θ, ϕ connected with the cartesian ones through the relations

$$\left\{ \begin{array}{ll} x = \frac{\alpha}{2}\sinh\mu\, \sin\theta\cos\phi & 0 \le \mu < \infty \\ y = \frac{\alpha}{2}\sinh\mu\, \sin\theta\sin\phi & 0 \le \theta \le \pi \\ z = \frac{\alpha}{2}\cosh\mu\, \cos\theta & 0 \le \phi < 2\pi \end{array} \right\} \quad (5)$$

where α stands for the focal distance. We start with the complete set of eigensolutions of Laplace operator, which are the regular harmonic functions at the origin

$$u^0_{nm}(\mathbf{r}) = P^m_n(\cosh\mu)P^m_n(\cos\theta)e^{im\phi}, \quad n = 0,1,2,\ldots, \quad |m| \le n \quad (6)$$

expressed in spheroidal coordinates, where we recognize the well known Legendre functions. We substitute every member of (6) in Eq.(3) aiming at constructing the corresponding eigensolution of Helmholtz equation. Then every harmonic function u^0_{nm} gives birth to the dynamic eigensolution

$$u_{nm}(\mathbf{r}) = P^m_n(\cosh\mu)P^m_n(\cos\theta)e^{im\phi} - \frac{kr}{2}\int_0^1 P^m_n(\cosh\mu')P^m_n(\cos\theta')e^{im\phi'}J_1(kr\sqrt{1-t})\sqrt{\frac{t}{1-t}}dt \quad (7)$$

In [Charalambopoulos and Dassios (2002)] it is proven that u_{nm} can be decomposed as:

$$u_{nm}(\mathbf{r}) = u^{(1)}_{nm}(\mathbf{r}) + u^{(2)}_{nm}(\mathbf{r}) \quad (8)$$

where

$$u^{(1)}_{nm}(\mathbf{r}) = P^m_n(\cosh\mu)P^m_n(\cos\theta)e^{im\phi} - \sum_{p=0}^{[\frac{n}{2}]}\sum_{l=0}^{[\frac{n-2p}{2}]} B_{n,m,p,l}P^m_{n-2p-2l}(\cosh\mu)P^m_{n-2p-2l}(\cos\theta)e^{im\phi} \quad (9)$$

$$u^{(2)}_{nm}(\mathbf{r}) = \sum_{p=0}^{[\frac{n}{2}]}\sum_{l=0}^{[\frac{n-2p}{2}]} B_{n,m,p,l}\Gamma\left(n-2p+\frac{3}{2}\right) \frac{J_{(n-2p+\frac{1}{2})}(kr)}{\left(\frac{kr}{2}\right)^{n-2p+1/2}}P^m_{n-2p-2l}(\cosh\mu)P^m_{n-2p-2l}(\cos\theta)e^{im\phi} \quad (10)$$

In the relations above, Γ stands for the well known Gamma function, while J is the Bessel function of first kind. In addition, the quantities $B_{n,m,p,l}$ are given by the relation

$$B_{n,m,p,l} = \left\{ \begin{array}{ll} \frac{(-1)^p(n+m)!(n-2p-2l-m)!(2n-2p)!}{(n-m)!(n-2p-2l+m)!p!} & |m| \le \kappa \\ \frac{(n-2p-l)!(2n-4p-4l+1)}{(n-p)!l!2^{2p+2l}(2n-4p-2l+1)!} & \\ 0 & |m| > \kappa \end{array} \right. \quad (11)$$

where $\kappa = n-2p-2l$ and constitute the expansion coefficients of the harmonic functions calculated at $\mathbf{r}' = t\mathbf{r}$ $(t \in [0,1])$ in terms of the same functions at $\mathbf{r}$, i.e.

$$P^m_n(\cosh\mu')P^m_n(\cos\theta')e^{im\phi} = \sum_{p=0}^{[\frac{n}{2}]}\sum_{l=0}^{[\frac{n-2p}{2}]} B_{n,m,p,l}t^{n-2p}P^m_{n-2p-2l}(\cosh\mu)P^m_{n-2p-2l}(\cos\theta)e^{im\phi} \quad (12)$$

The fourth of the authors of this work was not very attentive to remark in [Charalambopoulos and Dassios (2002)], that evoking Eq. (12) for $t = 1$ leads immediately to vanishing of $u^{(1)}_{nm}$ for every pair (n,m), and so only $u^{(2)}_{nm}$ participates in the formation of the eigensolutions u_{nm} of Helmholtz equation. Concequently

$$u_{nm}(\mathbf{r}) = \sum_{p=0}^{[\frac{n}{2}]}\sum_{l=0}^{[\frac{n-2p}{2}]} B_{n,m,p,l}\Gamma(n-2p+\frac{3}{2}) \frac{J_{(n-2p+\frac{1}{2})}(kr)}{(\frac{kr}{2})^{n-2p+1/2}}P^m_{n-2p-2l}(\cosh\mu)P^m_{n-2p-2l}(\cos\theta)e^{im\phi} \quad (13)$$

Representation (13) could be an elegant formula of $u_{nm}(\mathbf{r})$ if the radial coordinate r was not encountered therein. Actually the radial component r involves both spheroidal coordinates μ, θ and prevents $u_{nm}(\mathbf{r})$, in this form, from being expressible in terms of spheroidal coordinates separable manner. In [Charalambopoulos and Dassios (2002)] it is explained how this is affronted and how we obtain pure separable forms for the interior solutions of Helmholtz equation.

However, expression (13) is a very useful "hybrid" form of $u_{nm}(\mathbf{r})$ as it consists of a finite superposition of products. Each one of those products is built by a harmonic separable part and a wave term, incorporating the wave number k appropriately accompanied by the radial distance r. This expression is the convenient one for constructing the exterior eigensolutions of Helmholtz equation. We consider separately the functions generated by splitting $e^{im\phi}$ to its real and imaginary parts.

$$\begin{Bmatrix} u^c_{nm}(\mathbf{r}) \\ u^s_{nm}(\mathbf{r}) \end{Bmatrix} = \sum_{p=0}^{[\frac{n}{2}]} \sum_{l=0}^{[\frac{n-2p}{2}]} B_{n,m,p,l}\Gamma\left(n-2p+\frac{3}{2}\right) \frac{J_{(n-2p+\frac{1}{2})}(kr)}{\left(\frac{kr}{2}\right)^{n-2p+1/2}} P^m_{n-2p-2l}(\cosh\mu)P^m_{n-2p-2l}(\cos\theta) \begin{Bmatrix} \cos(m\phi) \\ \sin(m\phi) \end{Bmatrix} \quad (14)$$

We replace now in the formulae above, the Bessel function J with the corresponding outwards radiating Hankel one, via the relation $H_{n-2p+\frac{1}{2}}(kr) = J_{n-2p+\frac{1}{2}}(kr) + iY_{n-2p+\frac{3}{2}}(kr)$, constructing so the functions $\hat{u}^c_{nm}$ and $\hat{u}^s_{nm}$, which are irregular in the vicinity of $r=0$ and constitute candidates for being outgoing waves obeying to Helmholtz equation. We treat only $\hat{u}^c_{nm}$ for simplicity. It is preferable to work with the spherical Hankel functions instead of the cylindrical ones [Bell (1967)]. Then

$$\hat{u}^c_{nm}(\mathbf{r}) = \sum_{p=0}^{[\frac{n}{2}]} \sum_{l=0}^{[\frac{n-2p}{2}]} B_{n,m,p,l}\Gamma\left(n-2p+\frac{3}{2}\right) \frac{2}{\sqrt{\pi}} \frac{h^{(1)}_{n-2p}(kr)}{(\frac{kr}{2})^{n-2p}} P^m_{n-2p-2l}(\cosh\mu)P^m_{n-2p-2l}(\cos\theta) cos(m\phi) \quad (15)$$

For comparison, we express u^c_{nm} in terms of Spherical Bessel functions obtaining

$$u^c_{nm}(\mathbf{r}) = \sum_{p=0}^{[\frac{n}{2}]} \sum_{l=0}^{[\frac{n-2p}{2}]} B_{n,m,p,l}\Gamma\left(n-2p+\frac{3}{2}\right) \frac{2}{\sqrt{\pi}} \frac{j_{n-2p}(kr)}{(\frac{kr}{2})^{n-2p}} P^m_{n-2p-2l}(\cosh\mu) P^m_{n-2p-2l}(\cos\theta)cos(m\phi) \quad (16)$$

We consider the Rayleigh's formula [Bell (1967)]

$$h^{(1)}_n(z) = -i(-1)^n z^n \left(\frac{1}{z}\frac{d}{dz}\right)^n \left(\frac{e^{iz}}{z}\right), \quad (17)$$

based on which, we infer that the function

$$f^c_{nm}(k;\mathbf{r}) = k^{2n+1}(\Delta+k^2)\hat{u}^c_{nm}(\mathbf{r}) \quad (18)$$

considered as a function of k, where $\mathbf{r}\neq 0$ is kept fixed, is analytic in the upper half plane of the complex plane. The real part $\upsilon^c_{nm}(k;\mathbf{r})$ of $f^c_{nm}(k;\mathbf{r})$ is a harmonic function in its definition domain. On the real axis ($Im(k)=0$), we have

$$\begin{aligned} \upsilon^c_{nm}(k;\mathbf{r})|_{k\in R} &= Re\{k^{2n+1}(\Delta+k^2)\hat{u}^c_{nm}(\mathbf{r})\}|_{k\in R} \\ &= k^{2n+1}(\Delta+k^2)u^c_{nm}(\mathbf{r}) = 0 \end{aligned} \quad (19)$$

On the large semicircle of the upper half-plane of radius R, the harmonic function $\upsilon^c_{nm}(k;\mathbf{r})$ takes values decaying to zero for $R\to\infty$. This is proven by considering formula (17) and examining the asymptotic behavior of the crucial term e^{iz} for $z = Re^{i\gamma}r$ where $\arg\gamma \in (0,\pi)$.

Thus, the harmonic function $\upsilon^c_{nm}(k;\mathbf{r})$ vanishes in the upper half-plane and so does clearly the analytic function f^c_{nm}. Then for real k, $(\Delta+k^2)\hat{u}^c_{nm}(\mathbf{r}) = 0$ providing that $\hat{u}^c_{nm}$ belongs to $ker(\Delta+k^2)$. Similarly we treat $\hat{u}^s_{nm}(\mathbf{r})$ and finally obtain that all $\hat{u}_{nm}(\mathbf{r})$ constitute eigensolutions of the Helmholtz equation.

The radiating character of $\hat{u}_{nm}(\mathbf{r})$ is due to the asymptotic behavior of the Hankel function, revealing the usefulness of the "hybrid" representation introduced above, but this is going to be presented clearly in next section.

We are in position now to discuss the process of obtaining solutions in separable form. In [Charalambopoulos and Dassios (2002)], the solutions regular at origin are constructed in the following form

$$u_{nm}(\mathbf{r}) = \sum_{q=0}^{\infty} \sum_{j=0}^{q} \sum_{p=0}^{[\frac{n}{2}]} \sum_{l=0}^{[\frac{n-2p}{2}]} \sum_{i=-j}^{j} A(q,j,n,m,p,l,i,c) \left[(\sinh\mu)^{2q-2j} P^m_{n-2p-2l}(\cosh\mu)\right] P^m_{n-2p-2l+2i}(\cos\theta)e^{im\phi} \quad (20)$$

if Eq. (12) , with t=1, is taken into account. In Eq. (20) , $c=\frac{ka}{2}$ and $A(q,j,n,m,p,l,i,c)$ is a specific function of its arguments [Charalambopoulos and Dassios (2002)].

Consequently, the interior eigensolutions can be written in a quasi-separable form as every u_{nm} is a specific superposition of separable terms. The exterior eigensolutions $\hat{u}_{nm}$ are handled as follows. We remark that

$$\hat{u}_{nm}(\mathbf{r}) = u_{nm}(\mathbf{r}) + i\tilde{u}_{nm}(\mathbf{r}) \tag{21}$$

where $\tilde{u}_{nm}(\mathbf{r})$ is constructed with Bessel function of first kind in Eq.(13) replaced by the corresponding Neumann function. However, given that $Y_{n-2p+\frac{1}{2}}(kr) = (-1)^{n+1}J_{-n+2p-\frac{1}{2}}(kr)$ [Bell (1967)], we infer that

$$\tilde{u}_{nm}(\mathbf{r}) = \sum_{p=0}^{[\frac{n}{2}]}\sum_{l=0}^{[\frac{n-2p}{2}]} B_{n,m,p,l}\Gamma\left(n-2p+\frac{3}{2}\right) \frac{(-1)^{n+1}J_{(-n+2p-\frac{1}{2})}(kr)}{(\frac{kr}{2})^{n-2p+1/2}} P^m_{n-2p-2l}(\cosh\mu) P^m_{n-2p-2l}(\cos\theta)e^{im\phi} \tag{22}$$

According to the definition of Bessel function

$$\tilde{u}_{nm}(\mathbf{r}) = \sum_{q=0}^{\infty}\sum_{p=0}^{[\frac{n}{2}]}\sum_{l=0}^{[\frac{n-2p}{2}]} B_{n,m,p,l}\Gamma\left(n-2p+\frac{3}{2}\right) (-1)^{n+q+1}\frac{(\frac{c}{2})^{2(q-n+2p)-1}}{q!\Gamma(-n+2p+\frac{1}{2}+q)} \left(\sinh^2\mu+\cos^2\theta\right)^{q-n+2p-\frac{1}{2}} P^m_{n-2p-2l}(\cosh\mu) P^m_{n-2p-2l}(\cos\theta)e^{im\phi} \tag{23}$$

The crucial metric function $(\sinh^2\mu + \cos^2\theta)^{q-n+2p-\frac{1}{2}}$ is decomposed as follows:

$$\begin{aligned}&(\sinh^2\mu+\cos^2\theta)^{q-n+2p-\frac{1}{2}}\\ &=(\cosh^2\mu-\sin^2\theta)^{q-n+2p-\frac{1}{2}}\\ &=(\cosh\mu)^{2(q-n+2p)-1}\sum_{t=0}^{\infty}\frac{D_{q,n,p,t}}{t!}(-1)^t\left(\frac{\sin\theta}{\cosh\mu}\right)^{2t}\end{aligned} \tag{24}$$

where $D_{q,n,p,t} = (q-n+2p-\frac{1}{2})(q-n+2p-\frac{3}{2})\cdots(q-n+2p+\frac{1}{2}-t), t\geq 1, D_{q,n,p,0}=1$.

In addition,

$$\begin{aligned}&\sin^{2t}\theta P^m_n(\cos\theta)\\ &=\sum_{j=0}^{t}(-1)^j\binom{t}{j}\cos^{2j}\theta P^m_n(\cos\theta)\\ &=\sum_{j=0}^{t}(-1)^j\binom{t}{j}\sum_{i=-j}^{j}\beta^{m,j}_{n,i}P^m_{n+2i}(\cos\theta)\end{aligned} \tag{25}$$

where $\beta^{m,j}_{n,i}$ are the well defined expansion coefficients introduced in [Charalambopoulos and Dassios (2002)] and used in fact already in the construction of the coefficients $A(q,j,n,m,p,l,i,c)$ appeared in interior eigensolutions given by Eq. (20) . Consequently, the functions $\tilde{u}_{nm}$ defined by Eq. (22) obtain the quasi-separable form (i.e. expansion in term of separable terms)

$$\tilde{u}_{nm}(\mathbf{r}) = \sum_{q=0}^{\infty}\sum_{t=0}^{\infty}\sum_{j=0}^{t}\sum_{p=0}^{[\frac{n}{2}]}\sum_{l=0}^{[\frac{n-2p}{2}]}\sum_{i=-j}^{j}\tilde{A}(q,t,j,n,m,p,l,i,c) \left[(\cosh\mu)^{2(q-n+2p-t)-1}P^m_{n-2p-2l}(\cosh\mu)\right] P^m_{n-2p-2l+2i}(\cos\theta)e^{im\phi} \tag{26}$$

with

$$\tilde{A}(q,t,j,n,m,p,l,i,c) = B_{n,m,p,l}\Gamma(n-2p+\frac{3}{2}) (-1)^{n+q+1+j+t}\frac{(\frac{c}{2})^{2(q-n+2p)-1}}{q!\Gamma(-n+2p+\frac{1}{2}+q)j!(t-j)!} D_{q,n,p,t}\beta^{m,j}_{n-2p-2l,i} \tag{27}$$

Comparing Eqs. (20) with (26) , we infer that the eigensolutions constructed via the Neumann function, have additional complexity due to the presence of two infinite summations instead of one, and this is assigned to the separation of the fractional powers of the metric function $(\sinh^2\mu + \cos^2\theta)$. Combining Eqs. (13) and (21) we are in position to separate coordinates in the expression (21) representing the outwards radiating eigensolutions of Helmholtz equation. Several issues could emerge concerning functional theoretic properties of those functions apart from the mentioned regularity and propagation properties. We pay attention here, on the most important property concerning completeness of the

constructed solution set, since the purpose is to expand our arbitrary Helmholtz equation solution to this basic solutions set. The argument we present is purely qualitative and reveals the potential of Vekua transform. More precisely, every Helmholtz kernel space element has a unique potential conjugate via the inverse vekua tranform. Expanding this harmonic function in terms of the complete set of potential basic eigensolutions and taking the direct Vekua transformation to this expansion, we establish the sought ability to represent dynamic arbitrary solutions in terms of the constructed Vekua dynamic eigensolutions.

3 Investigation of the Scattering Problem

We consider a prolate spheroidal acoustically impenetrable scatterer occupying a specific region in R^3, defined by the scatterers's surface S, represented by the spheroidal surface

$$\mu = \mu_0 \tag{28}$$

The exterior region of the scatterer is denoted by D and is characterized by the range $\mu > \mu_0$, $0 \leq \theta \leq \pi$, $0 \leq \phi < 2\pi$ of spheroidal coordinates. The scatterer is illuminated by a time harmonic incident accoustic plane-wave, with frequency ω. Suppressing the time dependence $e^{-i\omega t}$ in all the physical quantities of the scattering process, the incident field is represented by the time reduced plane wave

$$u^{inc}(\mathbf{r}) = e^{i\mathbf{kr}}, \mathbf{r} \in D \tag{29}$$

where $\mathbf{k} = k\hat{\mathbf{k}}$, k is the wavenumber of the process and $\hat{\mathbf{k}}$ is the direction of the incident field. The scatterer reacts to the plane wave propagation, producing a secondary acoustic field, the scattered one, denoted by u^{sc}, which satisfies exactly like the incident wave, the Helmholtz equation

$$\Delta u^{sc}(\mathbf{r}) + k^2 u^{sc}(\mathbf{r}) = 0, \ \mathbf{r} \in D \tag{30}$$

This field emanates from the scatterer and radiates to infinity, satisfying uniformly over all directions, the well known Sommerfeld radiation condition

$$\frac{\partial u^{sc}(\mathbf{r})}{\partial r} - iku^{sc}(\mathbf{r}) = O(\frac{1}{r^2}), \ r \to \infty \tag{31}$$

The total field $u(\mathbf{r}) = u^{inc}(\mathbf{r}) + u^{sc}(\mathbf{r})$ defined in $\overline{D} = D \cup S$, obeys, on scatterer's surface, to a specific type of boundary condition, depending on the special nature of the scatterer. We focus on the soft scatterer case implying that

$$u(\mathbf{r}) = u^{inc}(\mathbf{r}) + u^{sc}(\mathbf{r}) = 0, \mathbf{r} \in S \tag{32}$$

The methodology suggested here, is based on exploiting the eigensolutions constructed in the previous section. More precisely, these eigensolutions are produced via the vekua transformation of the complete set of the spheroidal harmonic separable solutions. From all these transformed fundamental solutions, we select the set of outgoing radiating fields, since only these functions satisfy radiation condition (31) . We expand then, the unknown scattered field in terms of the aforementioned radiating basic solutions to obtain

$$u^{sc}(\mathbf{r}) = \sum_{n=0}^{\infty} \sum_{m=-n}^{n} A_{nm} \hat{u}_{nm}(\mathbf{r}), \mathbf{r} \in D, \tag{33}$$

where the coefficients A_{nm} absorb the unknown character of $u^{sc}(\mathbf{r})$.

The representation (33) can be exploited to provide the far-field pattern, which determines the behavior of the scattered field far-away the scatterer and constitutes usually the measured quantity in direct scattering. What is necessary, is to investigate the asymptotic behavior (for r$\to \infty$) of the eigensolutions $\hat{u}_{nm}(\mathbf{r})$. In the realm of large r>>1, we apply an extended, but straightforward asymptotic analysis of the special functions involved in the "hybrid" definition formula of $\hat{u}_{nm}(\mathbf{r})$, i.e. in

$$\hat{u}_{nm}(\mathbf{r}) = \sum_{p=0}^{[\frac{n}{2}]} \sum_{l=0}^{[\frac{n-2p}{2}]} B_{n,m,p,l} \Gamma\left(n-2p+\frac{3}{2}\right) \frac{H^{(1)}_{(n-2p+\frac{1}{2})}(kr)}{(\frac{kr}{2})^{n-2p+1/2}} P^m_{n-2p-2l}(\cosh\mu) P^m_{n-2p-2l}(\cos\theta) e^{im\phi} \tag{34}$$

More precisely, following [Lebedev (1972)]

$$H_\nu^{(1)}(kr)=\left(\frac{2}{\pi kr}\right)^{\frac{1}{2}}e^{i\left[kr-\frac{1}{2}\nu\pi-\frac{1}{4}\pi\right]}$$
$$\left[\sum_{s=0}^{n}\frac{(\frac{1}{2}-\nu)_s(\frac{1}{2}+\nu)_s}{s!}(2ikr)^{-s}+O\left(\frac{1}{(kr)^{n+1}}\right)\right] \quad (35)$$

for $kr\gg 1$, i.e. for r large compared with the wavelength, which is the physical characteristic length. We remind the Pochhammer's symbol $(z)_n$ definition [Abramowitz and Stegun (1972)]

$$(z)_n=z(z+1)(z+2)...(z+n-1)=\frac{\Gamma(z+n)}{\Gamma(z)}$$

In addition, if r is large compared with the geometric characteristic length of the semiaxis, we have $r>>\frac{\alpha}{2}$ and then $\frac{r}{(\frac{\alpha}{2})}=\sqrt{\cosh^2\mu-\sin^2\theta}\simeq\cosh\mu\simeq\frac{1}{2}e^{\mu}>>1$. Then the involved Legendre polynomials in Eq.(34) behave as

$$P_\nu^m(\cosh\mu)\simeq P_\nu^m\left(\frac{e^\mu}{2}\right)$$
$$=\left(\frac{e^\mu}{2}\right)^\nu\frac{(2\nu)!}{2^\nu\nu!(\nu-m)!}+O\left(e^{\mu(\nu-1)}\right),\ \mu\to\infty \quad (36)$$

Replacing these expressions in formula (34) , we obtain after some straightforward manipulations that

$$\hat{u}_{nm}(\mathbf{r})=\frac{1}{\sqrt{\pi}}\frac{2}{kr}e^{-i\frac{\pi}{4}}e^{ikr}$$
$$\sum_{p=0}^{[\frac{n}{2}]}B_{n,m,p,0}\Gamma\left(n-2p+\frac{3}{2}\right)e^{-i\frac{1}{2}(n-2p+\frac{1}{2})\pi}\left(\frac{4}{k\alpha}\right)^{n-2p}$$
$$\frac{[2(n-2p)]!}{2^{n-2p}(n-2p)!(n-2p-m)!}P_{n-2p}^m(\cos\theta)e^{im\phi}$$
$$+O\left(\frac{1}{r^2}\right),\ r\to\infty. \quad (37)$$

Substituting the assymptotic expressions Eq. (37) in Eq. (33) we find that in the far-field region

$$u^{sc}(\mathbf{r})=\frac{e^{ikr}}{kr}f_\infty(\theta,\phi)+O(\frac{1}{r^2}),r\to\infty \quad (38)$$

where the far-field pattern $f_\infty(\theta,\phi)$ is given by

$$f_\infty(\theta,\phi)=\sum_{n=0}^{\infty}\sum_{m=-n}^{n}\frac{2}{\sqrt{\pi}}e^{-i\frac{\pi}{4}}A_{nm}$$
$$\sum_{p=0}^{[\frac{n}{2}]}B_{n,m,p,0}\Gamma\left(n-2p+\frac{3}{2}\right)e^{-i\frac{1}{2}(n-2p+\frac{1}{2})\pi}\left(\frac{4}{k\alpha}\right)^{n-2p}$$
$$\frac{2^{2p-n}[2(n-2p)]!}{(n-2p)!(n-2p-m)!}P_{n-2p}^m(\cos\theta)e^{(im\phi)} \quad (39)$$

The satisfaction of the boundary condition (32) leads to the determination of the expansion coefficients appeared in Eq (33) and hence to the solution of the direct scattering problem. In other words the well posed boundary value problem consisting of Eqs.(30),(31), (32) is reduced to determine the coefficients A_{nm} from the equation

$$\sum_{n=0}^{\infty}\sum_{m=-n}^{n}A_{nm}\hat{u}_{nm}(\mathbf{r})=-e^{i\mathbf{kr}},\ \mathbf{r}\in D \quad (40)$$

There exist several approaches appropriate to treat the boundary condition (40) . In order to comment on them, we evoke here the results of the previous section providing the basic eigensolutions $\hat{u}_{nm}(\mathbf{r})$ which are written here in the following more condensed form,

$$\hat{u}_{nm}(\mathbf{r})=\sum_{q=0}^{\infty}\sum_{p=0}^{[\frac{n}{2}]}\sum_{l=0}^{[\frac{n-2l}{2}]}P_{n-2p-2l}^m(\cosh\mu)$$
$$\left\{\sum_{j=0}^{q}\sum_{i=-j}^{j}A_1(q,j,n,m,p,l,c)(\sinh\mu)^{2q-2j}\right.$$
$$\beta_{n-2p-2l,i}^{m,j}P_{n-2p-2l+2i}^m(\cos\theta)e^{im\phi}$$
$$+i\sum_{t=0}^{\infty}\sum_{j=0}^{t}\sum_{i=-j}^{j}\tilde{A}_1(q,t,j,n,m,p,l,c)$$
$$(\cosh\mu)^{2(q-n+2p-t)-1}\beta_{n-2p-2l,i}^{m,j}P_{n-2p-2l+2i}^m(\cos\theta)$$
$$\left.e^{im\phi}\right\} \quad (41)$$

where the subscript "1" indicates the corresponding function divided by $\beta_{n,i}^{m,j}$. (We mention that the coefficients $A,\tilde{A}$ are proportional to $\beta_{n-2p-2l,i}^{m,j}$ as can be deduced from [Charalambopoulos and Dassios (2002)] and previous section).

On scatterer's surface, we have $\mu = \mu_0$ and clearly the basis functions $\hat{u}_{nm}(\hat{\mathbf{r}}) = \hat{u}_{nm}(\mu_0, \theta, \phi)$ depend only on θ, ϕ through the well known family of spherical harmonics $P_n^m(\cos\theta)e^{im\phi}$. So, one is tempted to handle (40) by "projecting" the equation on these spherical harmonics and simultaneously truncating the infinite sum suitably to construct a sequence of linear algebraic systems, whose solvability and solution convergence investigation should be the necessary steps towards a thorough estimation of the sought expansion coefficients. The elements of the so constructed algebraic systems matrix can be calculated analytically, easily, since as can be deduced immediately from Eq. (41) , the determination of inner products $\int_0^\pi \int_0^{2\pi} \hat{u}_{nm}(\mu_0, \theta, \phi) P_{n'}^{m'}(\cos\theta) e^{-im'\phi} \sin\theta d\theta d\phi$ degenerates to the well known orthogonality pairs $\int_0^\pi \int_0^{2\pi} P_{n-2p-2l+2i}^m(\cos\theta) P_{n'}^{m'}(\cos\theta) e^{i(m-m')\phi} \sin\theta \, d\theta d\phi$. However the so produced matrix lacks the symmetry property, which is proved to be useful in treating linear systems of first kind generated by truncation processes. We are going to suggest two alternative approaches. One of them is based on minimization principles, assuring the aforementioned symmetry and the second one is the simplest possible methodology if the requirement of symmetry is not adopted.

4 The Collocation and L^2 method for the solution of the scattering problem

The arguments presented in the last paragraph of previous section are exploited herein, to the formulation of appropriate schemes for the determination of the coefficients of the expansion of the scattered field, in terms of the radiating eigensolutions. We start both approaches by truncating the expansion of the scattered field to level N and defining the error function

$$\begin{aligned}\varepsilon_N(\theta,\phi) &= u_N^{sc}(\mathbf{r}) + u^{inc}(\mathbf{r})|_{\mathbf{r}\in S} \\ &= \sum_{n=0}^{N}\sum_{m=-n}^{n} A_{nm}\hat{u}_{nm}(\mu_0,\theta,\phi) + e^{i\mathbf{k}\cdot\mathbf{r}(\mu_0,\theta,\phi)} \end{aligned} \quad (42)$$

representing the failure of the satisfaction of the boundary condition due to truncation.

The L^2-approach suggests the minimization of the L^2-norm of this function, given by

$$\|\varepsilon_N\|_{L^2} = \left(\int_0^\pi \int_0^{2\pi} |\varepsilon_N(\theta,\phi)|^2 \sin\theta d\theta d\phi \right)^{1/2} \quad (43)$$

following the least squares framework methodology. It is clearly deduced that, minimizing the L^2-norm of the error in the surface of the scatterer, is equivalent to minimizing

$$\begin{aligned}\sum_{n,m}\sum_{n',m'} \Big[& A_{nm}\overline{A}_{n'm'}(\hat{u}_{nm},\hat{u}_{n'm'})_{L^2} + A_{nm}(\hat{u}_{nm}, e^{i\mathbf{k}\cdot()})_{L^2} \\ & + \overline{A}_{n'm'}(e^{i\mathbf{k}\cdot()},\hat{u}_{n'm'})_{L^2} + (e^{i\mathbf{k}\cdot()}, e^{i\mathbf{k}\cdot()})_{L^2} \Big] \end{aligned} \quad (44)$$

where $(,)_{L^2}$ indicates the usual L^2-inner product (with conjugation in the second term) in θ, ϕ space incorporating the weight function $sin\theta$, and $\sum_{n,m}$ stands for $\sum_{n=0}^{N}\sum_{m=-n}^{n}$ Minimizing expression (44) over the involved coefficients leads to the following linear system

$$\begin{aligned}\sum_{n',m'} (\hat{u}_{nm},\hat{u}_{n'm'})_{L^2}\overline{A}_{n'm'} + (\hat{u}_{nm}, e^{i\mathbf{k}\cdot()})_{L^2} = 0, \quad (45) \\ (n = 0,1,2,...,|m| \le n)\end{aligned}$$

Splitting every term in real and imaginary part, we obtain

$$\begin{aligned}(\hat{u}_{nm},\hat{u}_{n'm'})_{L^2} &= (u^c_{nm},u^c_{n'm'})_{L^2} + (u^s_{nm},u^s_{n'm'})_{L^2} \\ &+ (\tilde{u}^c_{nm},\tilde{u}^c_{n'm'})_{L^2}(\tilde{u}^s_{nm},\tilde{u}^s_{n'm'})_{L^2} \\ &+ (\tilde{u}^c_{nm},u^s_{n'm'})_{L^2} - (\tilde{u}^s_{nm},u^c_{n'm'})_{L^2} \\ &- (u^c_{nm},\tilde{u}^s_{n'm'})_{L^2} + (u^s_{nm},\tilde{u}^c_{n'm'})_{L^2} \\ &+ i\Big\{ (u^s_{nm},u^c_{n'm'})_{L^2} - (u^c_{nm},u^s_{n'm'})_{L^2} \\ &+ (\tilde{u}^s_{nm},\tilde{u}^c_{n'm'})_{L^2} - (\tilde{u}^c_{nm},\tilde{u}^s_{n'm'})_{L^2} \\ &+ (\tilde{u}^c_{nm},u^c_{n'm'})_{L^2} + (\tilde{u}^s_{nm},u^s_{n'm'})_{L^2} \\ &- (u^c_{nm},\tilde{u}^c_{n'm'})_{L^2} - (u^s_{nm},\tilde{u}^s_{n'm'})_{L^2} \Big\} \end{aligned} \quad (46)$$

and

$$\begin{aligned}&(\hat{u}_{nm}, e^{i\mathbf{k}\cdot()})_{L^2} = \\ &(u^c_{nm},\cos(\mathbf{k}\cdot()))_{L^2} + (u^s_{nm},\sin(\mathbf{k}\cdot()))_{L^2} \\ &- (\tilde{u}^s_{nm},\cos(\mathbf{k}\cdot()))_{L^2} + (\tilde{u}^c_{nm},\sin(\mathbf{k}\cdot()))_{L^2} \\ &+ i\Big\{ (u^s_{nm},\cos(\mathbf{k}\cdot()))_{L^2} - (u^c_{nm},\sin(\mathbf{k}\cdot()))_{L^2} \\ &+ (\tilde{u}^c_{nm},\cos(\mathbf{k}\cdot()))_{L^2} + (\tilde{u}^s_{nm},\sin(\mathbf{k}\cdot()))_{L^2} \Big\} \end{aligned} \quad (47)$$

$$A_{nm} = a_{nm} + ib_{nm} \tag{48}$$

we consider the basic matrix blocks

$$B_{nm}^{n'm'} = \begin{pmatrix} Re[(\hat{u}_{nm}, \hat{u}_{n'm'})_{L^2}] & Im[(\hat{u}_{nm}, \hat{u}_{n'm'})_{L^2}] \\ Im[(\hat{u}_{nm}, \hat{u}_{n'm'})_{L^2}] & -Re[(\hat{u}_{nm}, \hat{u}_{n'm'})_{L^2}] \end{pmatrix}$$

$$\underline{x}_{nm} = [a_{nm}\, b_{nm}]$$

$$\underline{b}_{nm} = [Re(\hat{u}_{nm}, e^{i\mathbf{k}\cdot()})_{L^2}, Im(\hat{u}_{nm}, e^{i\mathbf{k}\cdot()})_{L^2}]$$

Then the system (45) obtains the matrix form

$$D_N \underline{x}_N = -\underline{b}_N \tag{49}$$

$$D_N = \begin{pmatrix} B_{0,0}^{0,0} & B_{0,0}^{1,-1} & \cdots & B_{0,0}^{1,1} & \cdots & B_{0,0}^{N,-N} & \cdots & B_{0,0}^{N,N} \\ B_{1,-1}^{0,0} & B_{1,-1}^{1,-1} & \cdots & B_{1,-1}^{1,1} & \cdots & B_{1,-1}^{N,-N} & \cdots & B_{1,-1}^{N,N} \\ B_{1,0}^{0,0} & B_{1,0}^{1,-1} & \cdots & B_{1,0}^{1,1} & \cdots & B_{1,0}^{N,-N} & \cdots & B_{1,0}^{N,N} \\ B_{1,1}^{0,0} & B_{1,1}^{1,-1} & \cdots & B_{1,1}^{1,1} & \cdots & B_{1,1}^{N,-N} & \cdots & B_{1,1}^{N,N} \\ \vdots & \vdots & \vdots & \vdots & \ddots & \vdots & \ddots & \vdots \\ B_{N,-N}^{0,0} & B_{N,-N}^{1,-1} & \cdots & B_{N,-N}^{1,1} & \cdots & B_{N,-N}^{N,-N} & \cdots & B_{N,-N}^{N,N} \\ B_{N,-N+1}^{0,0} & B_{N,-N+1}^{1,-1} & \cdots & B_{N,-N+1}^{1,1} & \cdots & B_{N,-N+1}^{N,-N} & \cdots & B_{N,-N+1}^{N,N} \\ \vdots & \vdots & \vdots & \vdots & \ddots & \vdots & \ddots & \vdots \\ B_{N,N}^{0,0} & B_{N,N}^{1,-1} & \cdots & B_{N,N}^{1,1} & \cdots & B_{N,N}^{N,-N} & \cdots & B_{N,N}^{N,N} \end{pmatrix} \tag{50}$$

where

$$\underline{\mathbf{x}}_N = \left(\underline{x}_{0,0}\underline{x}_{1,-1}\underline{x}_{1,0}\underline{x}_{1,1}\cdots\underline{x}_{N,-N}\underline{x}_{N,-N+1}\cdots\underline{x}_{N,N}\right)^{\mathbf{T}} \tag{51}$$

$$\underline{\mathbf{b}}_N = \left(\underline{b}_{0,0}\underline{b}_{1,-1}\underline{b}_{1,0}\underline{b}_{1,1}\cdots\underline{b}_{N,-N}\underline{b}_{N,-N+1}\cdots\underline{b}_{N,N}\right)^{\mathbf{T}} \tag{52}$$

The matrix D_N is a $[2(N+1)^2 \times 2(N+1)^2]$ symmetric one consisting of inner products between the eigensolutions, and $\underline{b}_N$ is a $[2(N+1)^2 \times 1]$ column containing the inner products between the oscillating functions $\cos(\mathbf{k}\cdot\mathbf{r})$, $\sin(\mathbf{k}\cdot\mathbf{r})$ and the eigensolutions. The vector $\underline{x}_N$ contains the estimation of the first $(N+1)^2$ coefficients $A_{nm} = a_{nm} + ib_{nm}$, at the truncation level N.

The inner products between the eigensolutions can be determined via their definitions (20), (26) after executing the simple ϕ, θ necessary integration. As an example

$$(u_{nm}^c, u_{n'm'}^c)_{L^2} = \sum_{q,q'=0,0}^{\infty,\infty} \sum_{j,j'=0,0}^{q,q'} \sum_{p,p'=0,0}^{[\frac{n}{2}],[\frac{n'}{2}]} \sum_{l,l'=0,0}^{[\frac{n-2p}{2}],[\frac{n'-2p'}{2}]} \sum_{j,j'=-i,-i'}^{i,i'} A(q,j,n,m,p,l,i,c)A(q',j',n',m',p',l',i',c) \Big[(\sinh\mu_0)^{2(q+q')-2(j+j')} P_{n-2p-2l}^{m}(\cosh\mu_0) P_{n'-2p'-2l'}^{m}(\cosh\mu_0)\Big] \frac{2\pi(n-2p-2l+2i+m)!}{[2(n-2p-2l+2i)+1](n-2p-2l+2i-m)!} \delta_{n-2p-2l+2i}^{n'-2p'-2l'+2i'} \delta_m^{m'} \tag{53}$$

(where δ_j^i is the Kronecker symbol and $\sum_{a,a'=b,b'}^{c,c'} = \sum_{a=b}^{c} \sum_{a'=b'}^{c'}$)

All the inner products involved in D_N have similar forms, apparently cumbersome, but it is an outcome of our analysis that the involved sums converge rapidly, due mainly to the specific form of the involved function A. In fact, it can be easily shown that

$$B_{nm}^{n'm'} = \begin{pmatrix} 0 & 0 \\ 0 & 0 \end{pmatrix} if\ m \neq m' \tag{54}$$

since all eigensolutions inner products are proportional to $\delta_m^{m'}$. This fact simplifies drastically the form of the matrix D_N.

Similar expressions can be deduced for the non-homogeneous terms of the linear system under discussion. For instance, if we consider, for reasons of brevity the case $\mathbf{k} = k\hat{\mathbf{z}}$, then the first term of Eq. (47) is proved to be given by

$$(u_{nm}^c, \cos(\mathbf{k}\cdot())_{L^2} = 4\pi \sum_{t=0}^{\infty} \sum_{q=0}^{\infty} \sum_{j=0}^{q} \sum_{p=0}^{[\frac{n}{2}]} \sum_{l=0}^{[\frac{n-2p}{2}]} \sum_{i=-j}^{j} \frac{(-1)^t c^{2t}}{t!} A(q,j,n,0,p,l,i,c) \left[(\sinh\mu_0)^{2q-2j} P_{n-2p-2l}^{m}(\cosh\mu_0)\right] \beta_{n-2p-2l+2i,s}^{0,t} \delta_{n-2p-2l+2i+2s}^{0} \delta_m^0 \tag{55}$$

The role of $c = \frac{1}{2}ka$ (it is involved apart from explicitely, also in function A) is crucial in the convergence rate of the infinite sums. In the resonance region, only a few terms are necessary to establish convergence in Eq.(55). Furthermore, in next section, it will be explained how an alternative numerical scheme has been constructed leading to the determination of all the necessary surface integrals involving in system (49).

As will be shown in next section, the L^2-norm minimization approach just exposed, turns out to be very robust and provides extremely accurate results even for elongated spheroidal bodies.

If we are not interested in solving such extreme cases, then an alternative simple approach may be followed. This methodology belongs to the general framework of the collocation methods. Although it is far more sensitive to the semi-axes ratio variance, it is far more performent than the L^2 approach, as it does not involve expensive quadratures and it can easily handle spheroidal bodies with semi-axes ratio greater than 0.9. In the Collocation approach, an appropriately selected grid of collocation points is constructed on the spheroidal surface, at which the error function is forced to be exactly zero. Then the following system arises

$$C_N \underline{x}_N = -\underline{g}_N \tag{56}$$

where C_N has similar structure with D_N given by Eq.(50) with the only difference that the subblocks $B_{nm}^{n'm'}$ give their places to the new matrices $E_{nm}^{n'm'}$ with

$$E_{nm}^{n'm'} = \begin{pmatrix} Re[\hat{u}_{nm}(\mathbf{r}_{n'm'})] & Im[\hat{u}_{nm}(\mathbf{r}_{n'm'})] \\ Im[\hat{u}_{nm}(\mathbf{r}_{n'm'})] & -Re[\hat{u}_{nm}(\mathbf{r}_{n'm'})] \end{pmatrix} \tag{57}$$

and $\mathbf{r}_{n'm'}$ are the sampling points parametrized by the indeces n', m' having the same range with the pair (n,m). Finally the non-homogeneous-column $\underline{g}_N$ has the same structure of $\underline{b}_N$ with elements $\underline{b}_{nm}$ replaced by

$$\underline{g}_{nm} = [\cos(\mathbf{k}\cdot\mathbf{r}_{nm}), \sin(\mathbf{k}\cdot\mathbf{r}_{nm})] \tag{58}$$

5 Numerical Implementation

5.1 Assembly and Solvability of the System

The core of the numerical investigation of the present work concerns the assembly and solution of the linear systems, arising in both collocation and L^2 approaches. Those systems involve extremely ill-conditioned matrices with condition numbers ranging from 10^{10} to 10^{220} as it will be demonstrated in the sequel. For the numerical treatment of those system, we have developed both Mathematica [Wolfram Research (2004)] and C++ software. Arbitrary precision arithmetic in C++ was provided by ARPREC library [Bailey, Yozo, Li, and Thompson (2002)]. The implementations of special functions in C++ was based on [Press, Teukolsky, Vetterling, and Flannery (2002)], [Zhang and Jin (1996)] with the necessary modifications and tunning to the working precision. This involves recalculation of all the usual parameters and mathematical constants entering the definition of special functions to the desired precision and appropriate modifications of the source code of the special functions [Press, Teukolsky, Vetterling, and Flannery (2002)], [Zhang and Jin (1996)] in order to be evaluated to the sought precision.

Special care was taken such that both C++-Arprec and Mathematica implementations agree in the final results. We had to take into consideration, for instance, that C++ and Mathematica dispose different generators for the Legendre functions for arguments greater than unity. The results obtained by both C++ and Mathematica implementations agreed to all but the last two decimal digits in any desired precision.

Special attention has been paid, in the framework of the collocation approach, to generate an appropriate grid of points on the scatterer's surface at which the boundary conditions should be fulfilled. The reason is that due to symmetries and involved periodicity of the vekua basis functions, the generation of points on the prolate spheroidal surface, in an equally spaced grid, results in a singular matrix. To remedy such issues, we employed a "random" point selection. More precisely, we generated a non regular grid using congruential random

number generators [Press, Teukolsky, Vetterling, and Flannery (2002)] for the selection of the angle pair (θ_i, ϕ_i) characterizing every point on the boundary.

For the solution of the linear systems we have used Singular Value Decomposition (SVD) which allows direct calculation of the condition number of the matrices involved. The performance bottleneck of our approaches in contrast to classical numerical methods (Finite Elements, Finite Volumes, Finite Differences, Spectral Elements) and especially Boundary Element Method in scattering theory [Agnantiaris and Polyzos (2003)], [Qian, Han, and Atluri (2004)], [Qian, Han, Ufimtsev, and Atluri (2004)], [Tsai, Lin, Young, and Atluri (2006)] is the assembly of the linear system, and not its solution, and thus computational overhead associated with the choice of SVD over the classical LU decomposition was negligible.

In the scattering process under investigation we consider a spheroidal scatterer with large semiaxis whose reduced length is kept constant and equal to one, while the small semiaxis suitably varies to give birth to several aspect ratios. The excitation of the scattering mechanism has been accomplished with a plane wave corresponding to the wave number propagation vector $\mathbf{k} = 0.1\hat{\mathbf{x}} + 0.1\hat{\mathbf{y}} + 0.1\hat{\mathbf{z}}$ (in reduced units).

5.2 Condition Number

In Fig. 1 we plot the condition number of matrices arising from the collocation and L^2 approaches correspondingly, as a function of the truncation level of the series N. It is evident that the condition number in both cases, is established mainly by the truncation level of the series while the role of the aspect-ratio (a_R) of the scatterer is almost negligible.

In Fig. 2 we keep constant the aspect-ratio of the scatterer to 0.9 and we plot the condition number of the matrices obtained by both approaches as a function of the truncation level of the series N.

We observe that the matrices assembled with the collocation discretization are better conditioned than those obtain with the L^2 minimization approach by a factor approximately 10^{30}. Once "arbitrary precision" is available however, this is a small price to pay for the increased accuracy provided by the L^2 approach, which is approximately five orders of magnitude for the specific aspect-ratio, see Tab. 4 and Tab. 5.

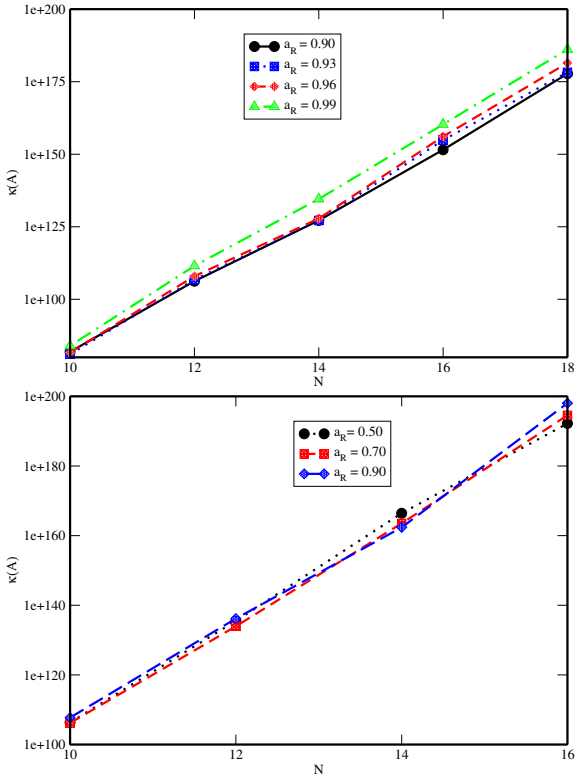

Figure 1: Condition number from collocation (upper) and L^2 (lower) approaches as a function of N for several a_R's.

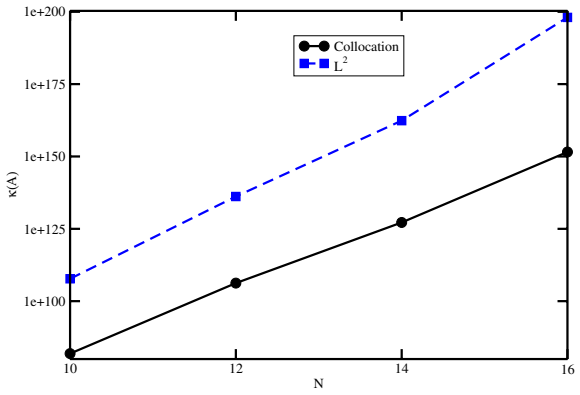

Figure 2: Condition number from L^2 and Collocation approaches as a function of N.

Due to the fact that those linear systems are highly ill-conditioned, the solution obtained by one backsubstitution is extremely inaccurate as we can see in Tab. 1. To adjust the solution to our working precision we used iterative refinement [Quarteroni, Sacco, and Saleri (2000)]. Error and residual bounds involved in iterative refinement procedure, are adjusted to the working precision. Below the desired precision was set to 128 digits and the update ($\|dx\|_2$) and residual ($\|r\|_2$) Euclidean norm tolerances were 10^{-128} and 10^{-129} respectively. The number of steps

Table 1: Solution using iterative refinement.

Iteration	$\|dx\|_2$	$\|r\|_2$
0	1.666402e-01	8.340997e-74
1	9.990374e-51	5.123128e-123
2	6.110645e-100	6.710668e-130
3	6.187603e-120	8.446949e-130

needed increases proportionally to the condition number. As a rule of thumb the working precision should be tunned to $\log_{10}\kappa(A)$ [Trefethen and Bau (1997)]. It is evident that in the first step of iterative refinement the norm of the solution update is still too large and unless several steps of iterative refinement are performed, we cannot obtain a reasonable solution to our system.

5.3 Convergence

The solution of the truncated linear systems fournishes the coefficients of the truncated scattered field. Using these coefficients, we construct an approximate scattered field, and validate the truncation level by investigating the error in the satisfaction of the boundary condition (32) , due to the replacement of the exact scattered field by the approximate one. This investigation has been implemented via two methods. We have studied the convergence in L^∞ and L^2-norms of the so constructed error function (42), defined as

$$\|\varepsilon_N\|_{L^\infty(S)} = \left(\operatorname*{ess\,sup}_S |\varepsilon_N|\right) = \max_S |\varepsilon_N| \tag{59}$$

$$\|\varepsilon_N\|_{L^2(S)} = \left(\int_S |\varepsilon_N|^2 \,\mathrm{d}S\right)^{\frac{1}{2}} \tag{60}$$

For the calculation and the visualization of the L^∞-norm we used a very dense regular grid of the prolate spheroidal surface. The error as given by Eq. 59 is calculated at all those points and the point where absolute value of the error attains its maximum, provides the value of discrete equivalent L^∞-norm. For studying the distribution of the error we visualized both its real and imaginary parts on the scatterer itself as a function of the azimuthal and polar angles. Computation of the integrals related to the L^2-norm was performed using Gauss-Legendre quadrature [Press, Teukolsky, Vetterling, and Flannery (2002)]. The number of the required quadrature points was adjusted such that the L^2-norm of the error converges to the fifth significant digit.

We examine the convergence of both approaches in the appropriate norms, as a function of the truncation level of the series, for various aspect ratios of the prolate spheroidal scatterer. We start by the collocation approach which is presented in Fig. 3.

It is evident that in this case, the role of the aspect-ratio of the scatterer is as significant as that of the truncation level of the series. In contrast to the previous study, where its role to the determination of the condition number was negligible, we observe that for aspect-ratios around 0.90 the convergence of the method slows down significantly and only marginally depends on the truncation level N.

In Fig. 4, we plot the dependence on the truncation level N, for various aspect-ratios, of the L^∞-norm of the real and imaginary parts of the error ε in the L^2 method framework, while in Fig. 5 we plot $\|\varepsilon\|_{L^2}$ obtained by the same approach.

The convergence here obviously deteriorates with smaller aspect ratios as it also happens with the collocation method. However it is clear that the range of aspect ratios the L^2 approach can handle, is amazingly wider. The rate of convergence of the logarithm of all the error norms, obtained by the L^2 approach is surpisingly linear. This simplifies significantly the regression analysis, for ob-

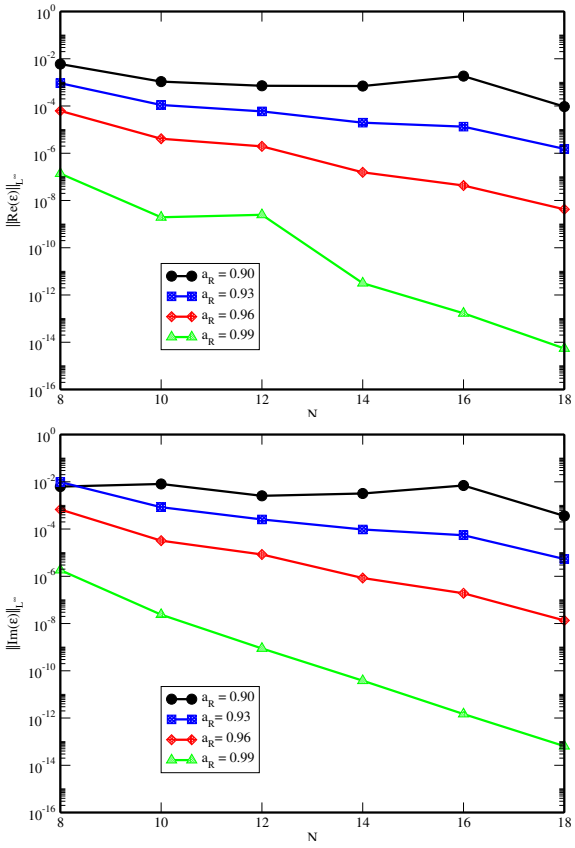

Figure 3: $\|Re(\varepsilon)\|_{L^\infty}$ and $\|Im(\varepsilon)\|_{L^\infty}$ in Collocation method as a function of N for various aspect ratios.

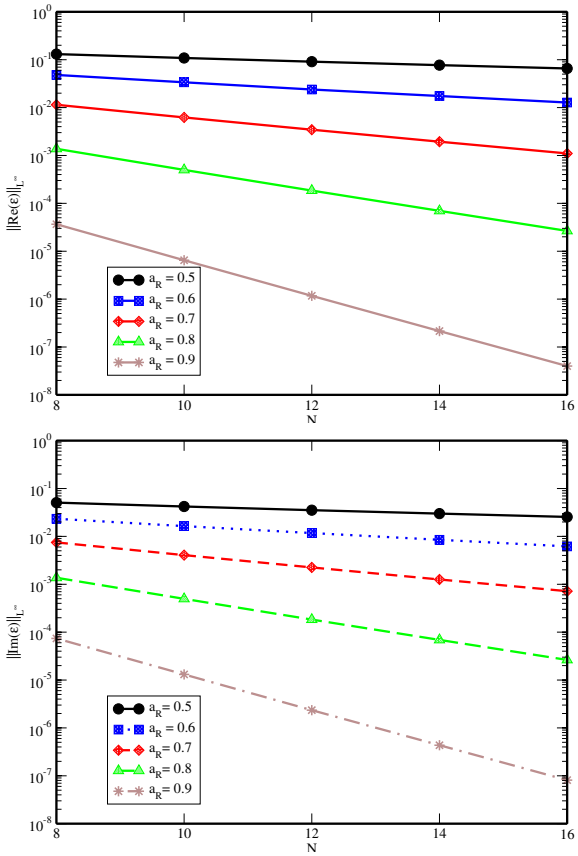

Figure 4: $\|Re(\varepsilon)\|_{L^\infty}$ and $\|Im(\varepsilon)\|_{L^\infty}$ in L^2 method as a function of N for various aspect ratios.

taining a formula describing the dependence of $\|\varepsilon\|_{L^2}$, on the aspect ratio of the scatterer and the truncation level of the series. This linearity can be expressed by the formula

$$\ln(\|\varepsilon\|_{L^2}) = C(a_R)N + D(a_R) \tag{61}$$

where C, D are functions depending only on the aspect ratio of the scatterer. The values of C, D for various aspect ratios are summarized in Tab. 2. For their determination we used the values of the error norms obtained by the L^2 approach summarized in Tab. 5. The dependence of $D(a_R)$ on a_R is linear as well, with regression coefficient (slope) equal to - 2.7081 and regression constant (intercept) equal to -0.23797. The dependence of $C(a_R)$ on a_R is plotted in Fig. 6. It is clearly nonlinear which gradually approaches zero. We are in position to describe this dependence with correlation coefficient 0.9999 using the following formula

$$C(a_R) = c_1 - c_2 e^{c_3(a_R - c_4)} \tag{62}$$

where c_1, c_2, c_3, c_4 are adjustable constant parameters. The values of the parameters obtained by the non-linear curve fit are presented in Tab. 3.

In Fig. 7, we visualize the real and imaginary parts of the error obtained with collocation approach on the (ϕ, θ) plane with $\phi \in [0, 2\pi)$, and $\theta \in [0, \pi]$. The aspect ratio of the scatterer is 0.9 and the truncation level was set to $N = 18$. Figures 8, 9, accompany the (ϕ, θ) plots to provide a detailed description of the error distribution. Figures 10 and 11 visualize both real and imagine parts of the error from the L^2 approach for a scatterer with aspect ratio 0.5 and truncation level $N = 18$.

Table 2: $C(a_R)$ and $D(a_R)$

a_R	$C(a_R)$	$D(a_R)$
0.5	-0.11505	-1.5731
0.6	-0.20107	-1.8566
0.7	-0.32968	-2.1610
0.8	-0.53157	-2.4441
0.9	-0.89035	-2.6334

Table 3: Non-linear curve fit constants.

c_1	$6.839 \cdot 10^{-5}$
c_2	0.161791
c_3	5.02222
c_4	0.56083

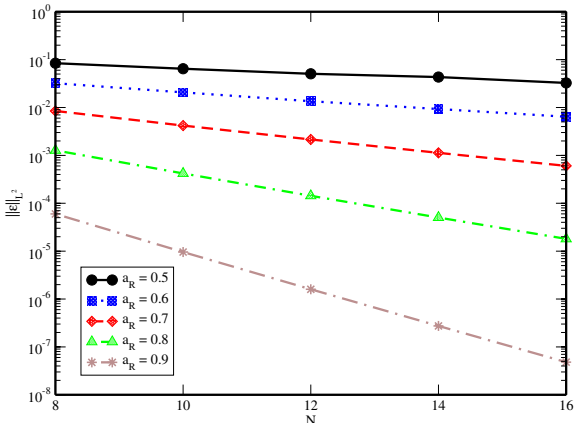

Figure 5: $\|\varepsilon\|_{L^2}$ obtained by L^2 approach as a function of N for various aspect-ratios.

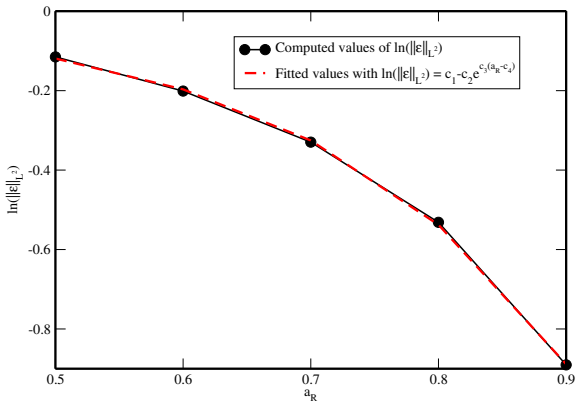

Figure 6: Fitted and computed values.

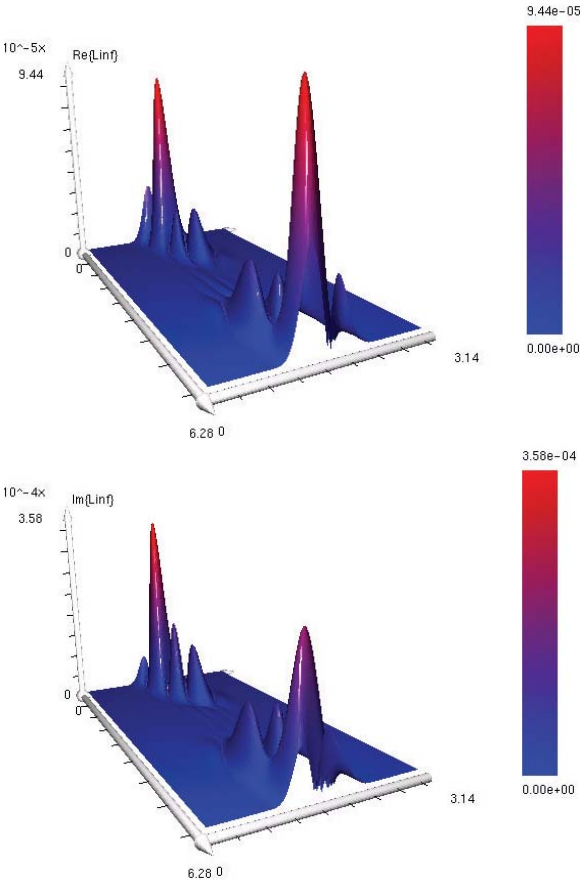

Figure 7: $Re(\varepsilon)$ and $Im(\varepsilon)$ in L^∞ method at aspect ratio 0.90 at truncation level N=18.

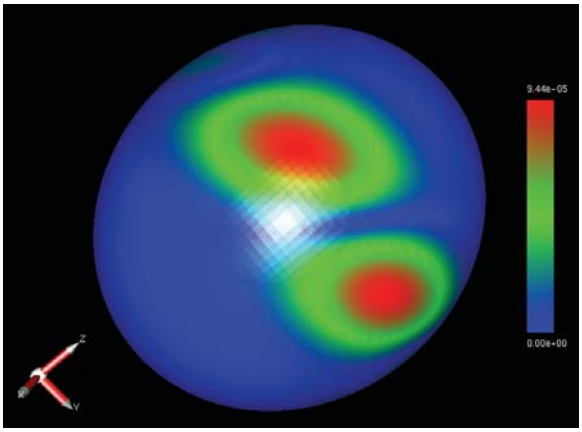

Figure 8: 3D plot of $Re(\varepsilon)$ at aspect ratio 0.90 at truncation level N=18 (Collocation Method).

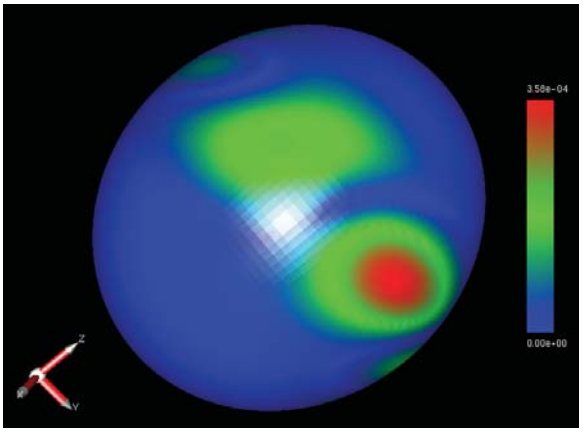

Figure 9: 3D plot of $Im(\varepsilon)$ at aspect ratio 0.90 at truncation level N=18 (Collocation Method).

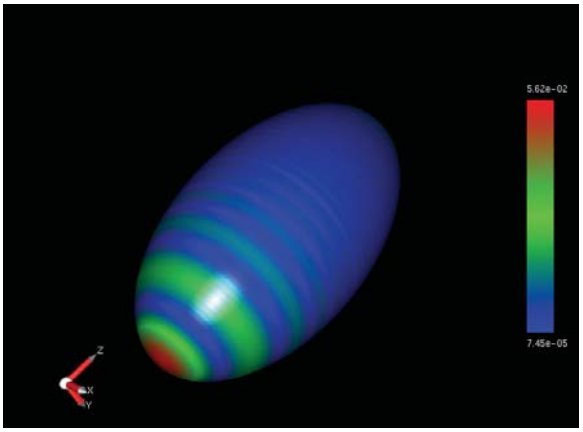

Figure 10: 3D plot of $Re(\varepsilon)$ at aspect ratio 0.50 at truncation level N=18 (L^2 method).

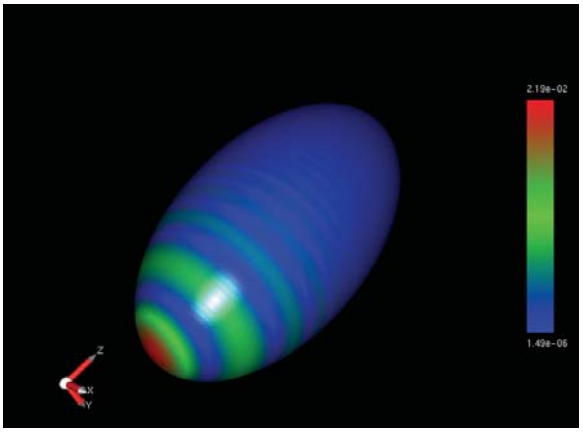

Figure 11: 3D plot of $Im(\varepsilon)$ at aspect ratio 0.50 at truncation level N=18 (L^2 method).

Table 4: Error norms (Collocation method)

$\mathbf{a}_R$	N	$\|Re\{\varepsilon\}\|_{L^\infty}$	$\|Im\{\varepsilon\}\|_{L^\infty}$	$\|\varepsilon\|_{L^2}$
0.90	16	1.8431e-3	6.9624e-3	4.8992e-3
	18	9.4445e-5	3.5835e-4	1.5952e-4
	20	2.9190e-5	1.1434e-4	6.2613e-5
0.91	16	3.1972e-4	1.2407e-3	8.8066e-4
	18	2.6764e-5	9.9460e-5	4.5527e-5
	20	7.6146e-6	2.9449e-5	1.6011e-5
0.92	16	6.5676e-5	2.6161e-4	1.8767e-4
	18	6.8419e-6	2.4772e-5	1.1722e-5
	20	1.7691e-6	6.9089e-6	3.6575e-6
0.93	16	1.3360e-5	5.4589e-5	3.9676e-5
	18	1.5305e-6	5.3694e-6	2.6428e-6
	20	3.5403e-7	1.4014e-6	7.2211e-7
0.94	16	2.4611e-6	1.0311e-5	7.6150e-6
	18	2.8629e-7	9.6558e-7	4.9977e-7
	20	5.8098e-8	2.3444e-7	1.1746e-7
0.95	16	3.7795e-7	1.6256e-6	1.2213e-6
	18	4.1770e-8	1.3397e-7	7.4262e-8
	20	7.2820e-9	3.0258e-8	1.4631e-8
0.96	16	4.2980e-8	1.9040e-7	1.4617e-7
	18	4.2283e-9	1.3474e-8	7.8024e-9
	20	6.1197e-10	2.6538e-9	1.2367e-9
0.97	16	2.9469e-9	1.4153e-8	1.0732e-8
	18	2.3816e-10	9.1159e-10	4.8052e-10
	20	2.7100e-11	1.2582e-10	5.6887e-11
0.98	16	7.7111e-11	4.3541e-10	3.1582e-10
	18	4.5167e-12	2.4106e-11	1.1671e-11
	20	3.6901e-13	1.9464e-12	8.8264e-13
0.99	16	1.6798e-13	1.4764e-12	9.9074e-13
	18	5.4610e-15	6.4575e-14	3.1108e-14
	20	2.6998e-16	1.9304e-15	1.0411e-15

Table 5: Error norms (L^2 method)

$\mathbf{a}_R$	N	$\|Re\{\varepsilon\}\|_{L^\infty}$	$\|Im\{\varepsilon\}\|_{L^\infty}$	$\|\varepsilon\|_{L^2}$
0.50	16	6.5606e-2	2.5508e-2	3.2551e-2
	18	5.6217e-2	2.1874e-2	2.6582e-2
0.60	16	1.2751e-2	6.1860e-3	6.4097e-3
	18	9.3826e-3	4.5556e-3	4.4775e-3
0.70	16	1.1027e-3	7.1718e-4	6.0417e-4
	18	6.3258e-4	4.1187e-4	3.2843e-4
0.80	14	6.9655e-5	6.8857e-5	5.0315e-5
	16	2.6562e-5	2.6308e-5	1.8046e-5
0.90	14	2.1491e-7	4.3466e-7	2.7400e-7
	16	3.9934e-8	8.1110e-8	4.8071e-8

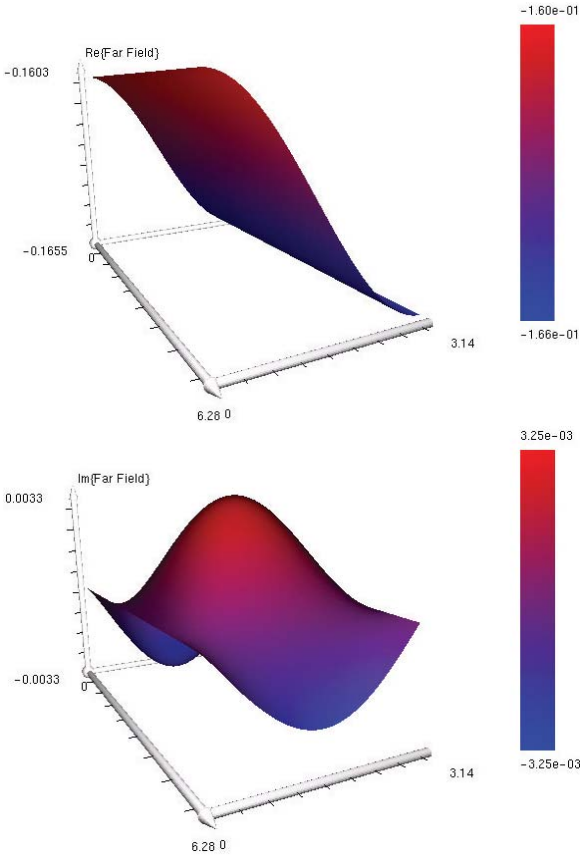

Figure 12: Real and Imaginary part of far field at aspect ratio 0.90 and truncation level $N = 18$.

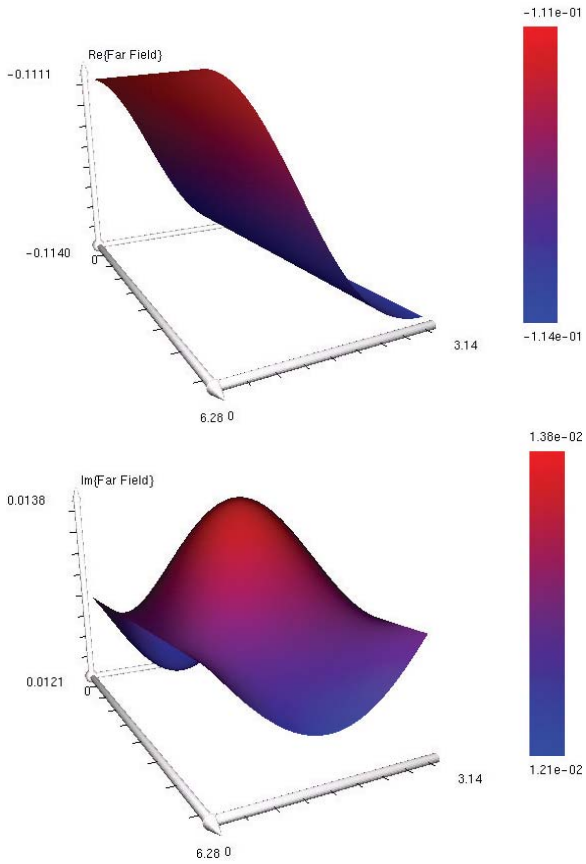

Figure 13: Real and Imaginary part of far field at aspect ratio 0.50 and truncation level $N = 18$.

5.4 Far Field

The far-field pattern constitutes the basic outcome of the analysis of the direct scattering problem. It is determined by Eq. 39 after having substituted the calculated expansion coefficients provided by the precending numerical process. In Figs. 12, 13 we visualize the real and imaginary part of the far-field pattern for the extreme elongated ($a_R = 0.5$) as well as for the prolate spheroid with $a_R = 0.9$.

Conclusions

In this paper, a new theoretical formulation for the solution of the acoustic scattering problem from prolate spheroidal scatterers has been developed. This new approach detours the well known spheroidal wave functions and their inherent numerical deficiencies. The essence of the proposed method is the extension of the well known Vekua transformation between the kernels of Laplace and Helmholtz equation to scattering problems. The starting point of determining the scattered field is to express it in terms of the constructed set of eigensolutions. The expansion coefficients constitute the unknown of our problem and solve a crucial linear system emergin from the boundary condition satisfaction. The next fundamental outcome of this work has been the thorough numerical investigation of this system given that the corresponding matrix is generally an extremely ill-conditioned one. The special feature of the numerical treatment is the development of arbitrary precision techniques to our problem. Two numerical schemes were suggested for the determination of the sought expansion coefficients, an error minimization and a collocation approach. The former obtains an optimal choice of the expan-

sion coefficients which minimizes the $\|\cdot\|_{L^2}$ norm of the error introduced in the satisfaction of the boundary condition, due to truncation. Although it is numerically intensive, it was proved to be a very robust and reliable scheme which could accurately handle very elongated prolate spheroidal scatterers. The second approach belongs to the wider class of collocation methods and provides a simple alternative, from an implementation point of view, when the spheroidal scatterers, under investigation, have aspect ratios not far from unity. We demonstrated that arbitrary precision arithmetic provides an indispensible tool for this type of problems as the condition numbers of the matrices obtained by both approaches is far beyond the one, that can be handled by conventional 64-bit and 80-bit IEEE floating point arithmetic formats.

Acknowledgement: All the computations have been performed in the Laboratory of Mathematical Modeling and Scientific Computing of the Materials Science Department using a Quad AMD Opteron. Additional computer resourses have been provided by the Research Center for Scientific Simulations (RCSS) of the University of Ioannina. For the 3D graphs we have used the visualization software *OPSIS* created by Drosos Kourounis.

References

Abramowitz, M.; Stegun, I. (1972): *Handbook of Mathematical Functions*. Dover.

Agnantiaris, J.; Polyzos, D. (2003): A boundary element method for acoustic scattering from non-axisymmetric and axisymmetric elastic shells . *CMES: Computer Modeling in Engineering & Sciences*, vol. 4, pp. 197–212.

Anagnostopoulos, K.; Mavratzas, S.; Charalambopoulos, A.; Fotiadis, D. (2003): Scattering of a spherical acoustic field from an eccentric spheroidal structure simulating the kidney-stone system. *Acta Mechanica*, vol. 161, pp. 39–52.

Bailey, D. H. (2004): High-Precision Floating-Point Arithmetic in Scientific Computation. *Lawrence Berkeley National Laboratory. Paper LBNL-57487. http://repositories.cdlib.org/lbnl/LBNL-57487.*

Bailey, D. H.; Yozo, H.; Li, X. S.; Thompson, B. (2002): ARPREC: An arbitrary precision computation package. *Lawrence Berkeley National Laboratory. Paper LBNL-53651. http://repositories.cdlib.org/lbnl/LBNL-53651.*

Barrowes, B.; O'Neil, K.; Grzegorczyk, T.; Kong, J. (2004): On the Assymptotic Expansion of the Spheroidal Wave Function and Its Eigenvalues for Complex Size Parameter. *Studies in Applied Mathematics*, vol. 113, pp. 271–301.

Bell, W. (1967): *Special functions for scientists and engineers*. D. Van Nostrand Company Ltd.

Borwein, J.; Bailey, D. (2004): *Mathematics by Experiment, Plausible Reasoning in the 21st Century*. A.K. Peters.

Charalambopoulos, A.; Dassios, G. (2002): On the Vekua Pair in Spheroidal Geometry ad its Role in Solving Boundary Value Problems. *Applicable Analysis*, vol. 81, pp. 85–113.

Charalambopoulos, A.; Dassios, G.; Fotiadis, D.; Massalas, C. (2001): Scattering of a point generated field by a multilayered spheroid. *Acta Mechanica*, vol. 150, pp. 107–119.

Charalambopoulos, A.; Dassios, G.; Perruson, G.; Lesselier, D. (2002): The Localized Nonlinear Approximation in Ellipsoidal Geometry. A Novel Approach to the Low-Frequency Scattering Problem. *Int. J. Eng. Sci.*, vol. 40, pp. 67–91.

Charalambopoulos, A.; Fotiadis, D.; Massalas, C. (2002): Scattering of a point generated field by kidney stones. *Acta Mechanica*, vol. 153, pp. 63–77.

Charalambopoulos, A.; Fotiadis, D. I.; Kourounis, D.; Massalas, C. (2001): On the solution of boundary value problems using spheroidal eigenvecto. *Computer Physics Communications*, vol. 139, pp. 153–171.

Kong, X. K.; Li, L. W.; Leong, M. S.; Kooi, P. S. (1999): A spheroidal vector wave function analysis of field and SAR distributions in a dielectric prolate spheroidal human head model, Progress in Electromagnetics research. *PIER*, vol. 22, pp. 149–179.

Kourounis, D.; Charalambopoulos, A.; Fotiadis, D. I. (2001): Human Head interaction with mobile phones:The spheroidal head model. *Proceedings of the Fifth International Workshop on Mathematical Methods in Scattering Theory and Biomedical Technology*.

Lebedev, N. N. (1972): *Special Functions and Their Applications*. Dover.

Li, L. W.; Kang, X.; Leong, M. (2001): *Spheroidal Wave Functions in Electromagnetic Theory*. Wiley Series in Microwave and Optical Engineering.

Perruson, G.; Lambert, M.; Lesselier, D.; Dassios, G.; Charalambopoulos, A. (2000): Electromagnetic Scattering by a tri-axial homogeneous penetrable ellipsoid:Low Frequency Derivation and Testing of the Localized Nonlinear Approximation. *Radio Science*, vol. 35, pp. 463–482.

Perruson, G.; Lesselier, D.; Lambert, M.; Bourgeois, B.; Charalambopoulos, A.; Dassios, G. (2000): Conductive Masses in a Half Space Earth in the Diffusive Regime :Fast Hybrid Modeling of a Low-Contrast Ellipsoid. *IEEE Transactions on Geoscience and Remote Sending*, vol. 38, pp. 1585–1599.

Press, W.; Teukolsky, S.; Vetterling, W.; Flannery, B. (2002): *Numerical Recipes in C++*. Cambridge University Press, 2nd Edition.

Qian, Z.; Han, Z.; Atluri, S. (2004): Directly derived non-hyper-singular boundary integral equations for acoustic problems, and their solution through Petrov-Galerkin schemes. *CMES: Computer Modeling in Engineering & Sciences*, vol. 5, pp. 541–562.

Qian, Z.; Han, Z.; Ufimtsev, P.; Atluri, S. (2004): Non-hyper-singular boundary integral equations for acoustic problems, implemented by the collocation-based boundary element method. *CMES: Computer Modeling in Engineering & Sciences*, vol. 6, pp. 133–144.

Quarteroni, A.; Sacco, R.; Saleri, F. (2000): *Numerical Mathematics*. Springer.

Shewchuk, R. (1997): Adaptive Precision Floating-Point Arithmetic and Fast Robust Geometric Predicates. *Discrete & Computational Geometry*, vol. 18, pp. 305–363.

Trefethen, L. N.; Bau, D. (1997): *Numerical Linear Algebra* . siam.

Tsai, C.; Lin, Y.; Young, D.; Atluri, S. (2006): Investigations on the accuracy and condition number for the method of fundamental solutions . *CMES: Computer Modeling in Engineering & Sciences*, vol. 16, pp. 103–114.

Vekua, I. (1942): Solutions of the Equation $\Delta u + \lambda^2 u = 0$. *Soobshcheniga Akademii Nauk Gruz. SSSR*, vol. 3, pp. 307–314.

Vekua, I. (1945): Inversion of an Integral Transformation and Some Applications. *Soobshcheniga Akademii Nauk Gruz. SSSR*, vol. 6, pp. 177–183.

Vekua, I. (1967): *New Methods for Solving Elliptic Equations*. North Holland Publishing Co.

Waterman, P. (1969): New formulation of acoustic scattering. *J. Acoust. Soc. Am.*, vol. 45, pp. 1417–1429.

Wolfram Research, I. (2004): Mathematica Edition: Version 5.1. *Wolfram Research, Inc.*

Zhang, H.; Han, Y. (2005): Scattering by a Confocal Multilayered Sphere Particle Illuminated by an Axial Gaussian Beam. *IEEE Transactions on antennas and propagation*, vol. 53, pp. 1514–1518.

Zhang, S.; Jin, J. (1996): *Computation of Special functions*. Wiley Interscience.